Acta Cryst. (1988). A**44**, 1073-1078

Quantitative Determination of Phases of X-ray Reflections from Three-Beam Diffractions. II. Experiments for Perfect Crystals

BY MAU-TSU TANG AND SHIH-LIN CHANG

Department of Physics, National Tsing Hua University, Hsinchu, Taiwan 30043

(*Received* 22 *March* 1988; *accepted* 22 *June* 1988)

Dedicated to Professor Ulrich Bonse on the occasion of his 60th birthday

Abstract

The method proposed by Chang & Tang [*Acta Cryst.* (1988). A**44**, 1065-1072] of quantitative determination of X-ray reflection phases from multiple diffraction profiles is applied to nearly perfect crystals of gallium arsenide. The detailed intensity-profile-analysis procedures are given. Multiple diffraction profiles obtained with a conventional X-ray source and synchrotron radiation are subjected to this analysis. It is found that, for this particular diffraction example, errors as small as 15° in phase determination are achieved. Errors due to the theoretical approximation, peak position measurement and scaling factor are also discussed.

I. Introduction

In the previous paper (Chang & Tang, 1988), hereafter referred to as paper I, we have derived, within the framework of the dynamical and kinematical theories of X-ray diffraction, the formalism for quantitative analysis of X-ray reflection phases from multiple diffraction intensity profiles. In that formalism, the kinematical diffraction intensity profile, which is phase independent, is subtracted from the total intensity profile. The remaining part of the profile, which is dynamical, provides the information about the phases. Moreover, the experimental parameters, such as instrumental broadening (beam divergence), and crystal mosaicity are taken into account.

In this paper we report experiments on multiple diffraction from nearly-perfect crystals. The detailed profile-analysis procedure, which leads to the experimental determination of X-ray reflection phases, is given. As a first step towards quantitative phase determination, we concentrate on perfect crystals of GaAs, where the known phases can be used for comparison with the experimentally determined phases.

II. Experimental

Two experimental set ups were used for obtaining multiple diffraction profiles; one with a conventional X-ray source and the other with synchrotron radiation.

The experimental arrangement with the conventional source is similar to the one reported by Renninger (1937). The set up consists of (1) an X-ray source, (2) a collimation system and (3) a four-circle semi-automatic single-crystal diffractometer (Huber 400). The X-rays were generated by an Elliott GX-21 rotating-anode generator. A Cu target and a filament of size 300×3000 μm were used. The generator was operating at 45 kV and 35 mA. An evacuated pipe with an exchangeable pinhole assembly at the exit end was used as the beam collimator. The focal size is about 300×300 μm. The beam divergences are 0·033 and 0·053°, in both vertical and horizontal directions, for pinholes of 480 μm (pinhole *A*) and 680 μm (pinhole *B*) in diameter, respectively. A schematic representation of this set up is shown in Fig. 1(*a*). The distances between the crystal, pinhole and source are also indicated in the same figure. Several [111]-cut plate-like GaAs crystals were used as the samples.

The experiment was performed by first aligning the crystal for the 222 reflection, the primary reflection *G*, and then by rotating it around the reciprocal-lattice vector **g** of the 222 reflection to bring additional sets

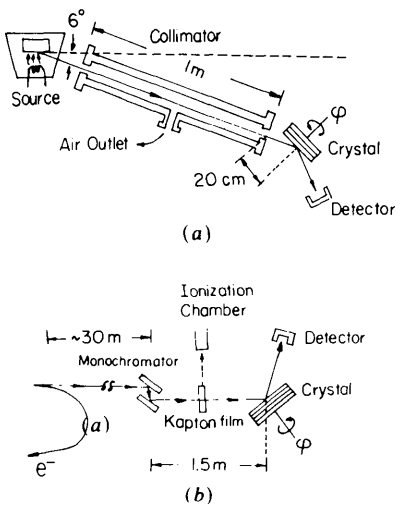

Fig. 1. Schematic representations of the experimental set ups with (*a*) conventional X-ray, (*b*) synchrotron radiation.

0108-7673/88/061073-06$03.00

of atomic planes (of the secondary reflection L) to satisfy Bragg's law. The interaction among the primary, the secondary and the incident beams modifies the intensity I_G of the primary 222 reflection. This intensity variation with respect to the two-beam intensity $I_{222}(2)$ *versus* the azimuthal angle φ of rotation forms a multiple diffraction profile. Fig. 2 is a 30° asymmetric portion of the multiple diffraction pattern. The mirrors occur at $\varphi = 0$ and $\varphi = 30°$, which correspond to the positions at which the vectors $[1\bar{1}0]$ and $[11\bar{2}]$ are coincident with the plane of incidence of the 222 reflection. Within this 30° range there are two four-beam and 14 three-beam *Umweganregung* reflections. The indices before and after the slashes represent the secondary reflection L and the coupling G-L, respectively. In order to obtain well resolved diffraction profiles, a slow azimuthal scan was employed. The profiles were later subjected to the profile analysis.

In the synchrotron radiation experiment, the five-circle single-crystal diffractometer (Kupčik, Wulf, Wendschuh, Wolf & Paehler, 1983) at Hasylab (Hamburg Synchrotron Laboratory), in DESY, Federal Republic of Germany, was used. The experimental set up is shown schematically in Fig. 1(*b*). The X-radiation was generated from the DORIS II storage ring, which was operating at 5 GeV and 20–40 mA in the single-bunch mode. A [111]-cut germanium double-crystal monochromator placed 30 m from the source was employed to tune the wavelength of the incident radiation. The intensity of Compton scattering of the incident beam from a Kapton film was monitored by an ionization chamber. This was used for intensity calibration. The crystal was mounted on a goniometer head attached to the five-circle diffractometer.

The crystal of GaAs was aligned for the 222 reflection using the centering process usually employed in single-crystal structure studies. Subsequently the crystal was subjected to a ψ scan (*International Tables for X-ray Crystallography*, 1974) around the reciprocal-lattice vector of the 222 reflection. Since the arcs of the goniometer head could not be adjusted by remote electronic control, exact azimuthal rotation around **g** could not be performed. It was therefore decided first to use the ψ scan to locate the peak position of a multiple reflection, and then perform the centering procedure to realign the crystal near the peak position. Finally a ψ scan was carried out again. In this way, well defined multiple diffraction intensity profiles were obtained.

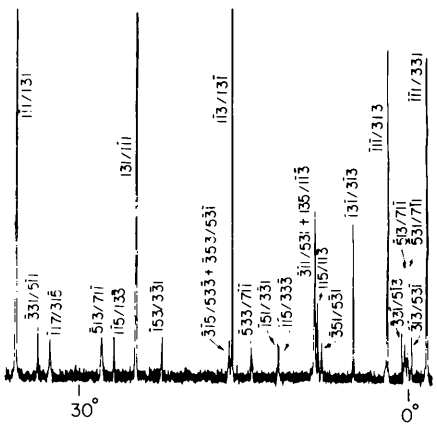

Fig. 2. Multiple diffraction pattern of GaAs (222) for Cu $K\alpha_1$ radiation.

III. Diffraction-profile analysis and phase determination

In paper I, it is suggested that the phase-dependent (dynamical) intensity profile can be obtained by subtracting the kinematical profile from the total experimental profile. Referring to equations (31) and (34) of paper I, we recall that the kinematical profile I_K is a Lorentzian, which is rewritten as

$$I_K = \frac{C_0 a_2(|F_{G-L}||F_{L-O}|/|F_{G-O}||F'_{O-O}|)^2(\eta_i/\eta_T)}{(\Delta\varphi + K^2\chi'_{O-O}/2W)^2 + (\eta_T/2)^2} \quad (1)$$

where the F's are the structure factors. η_i is the intrinsic kinematical peak width, which is equal to $|k^2\chi''_{O-O}/W + G_2|\chi_{O-O}|/W|$ according to equation (36) of paper I. The total peak width at half maximum is $\eta_T = \eta_i + \eta_B + \eta_M$. η_B and η_M are the instrumental broadening and the mosaic spread. a_2 is a geometric factor defined in equation (27) of paper I. C_0 is a scaling factor. It is determined in the following way. According to equation (26) of paper I, the relative total intensity I'_G is the sum of the kinematical intensity I_K, the dynamical I_d and the two-beam background for all the azimuthal poisitions $\Delta\varphi$, where

$$I_d = 2Pa_1 \cos u, \quad (2)$$

with

$$\cos u = [2(\Delta\varphi)\cos\delta - \eta_T \sin\delta]QW. \quad (3)$$

The quantities Q and W are defined in paper I. δ is the invariant phase which is equal to $\psi_{G-L} + \psi_{L-O} + \psi_{O-G}$. ψ_G is the phase of the G reflection. Since I_d is phase dependent, its value can be positive or negative depending on whether the phase is negative ($\sin\delta < 0$) or positive ($\sin\delta > 0$). The total intensity at the peak position $\Delta\varphi = 0$ is therefore increased for $\sin\delta < 0$ and decreased for $\sin\delta > 0$. This fact can be understood from equation (26) and the calculated intensities *versus* $\Delta\varphi$ shown in Fig. 3 of paper I. Based on this consideration, the experimental kinematical intensities can be determined from the averaged total intensities over all the involved three-beam cases, provided that these measured intensities are normalized to a common scale. This normalization is done by dividing the experimental intensities $I_P(E)$ at

$\Delta\varphi = 0$ by the calculated kinematic intensities I_K, namely, $I_P(E)/I_K$. Fig. 3 is such a plot for the three-beam cases obtained with the conventional source. The abscissa indicates the three-beam cases whose intensity measurements were carried out with the pinholes A and B. The average ratio $I_P(E)/I_K$, determined from the horizontal line, is the scaling factor, *i.e.* $C_0 = 0{\cdot}91$. For the synchrotron radiation experiment, the C_0 value is $C_0 = 3{\cdot}30$.

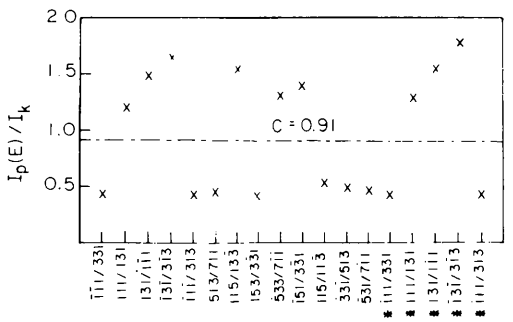

Fig. 3. Determination of the scaling factor C_0 for Cu $K\alpha_1$ (data obtained with pinhole B are marked by *).

Once the C_0 factors are determined, the Lorentzian forms of the kinematical profiles, I_K *versus* $\Delta\varphi$, can be constructed with their peak positions at φ(cal.), the calculated kinematical peak position. φ is determined from the geometry of multiple diffraction, *i.e.* $\varphi = \varphi_0 \pm \beta$ [(Cole, Chambers & Duun, 1962); see also the definitions for φ_0 and β given in paper I]. It should be noted that owing to the dynamical diffraction effect (the phase effect), the experimental peak position is shifted away from the calculated kinematical peak position ($\Delta\varphi = 0$). This shift, $\Delta\varphi$, can be determined experimentally.

Figs. 4 and 5 show the experimental profiles (solid curves), the kinematical Lorentzian profiles (dashed

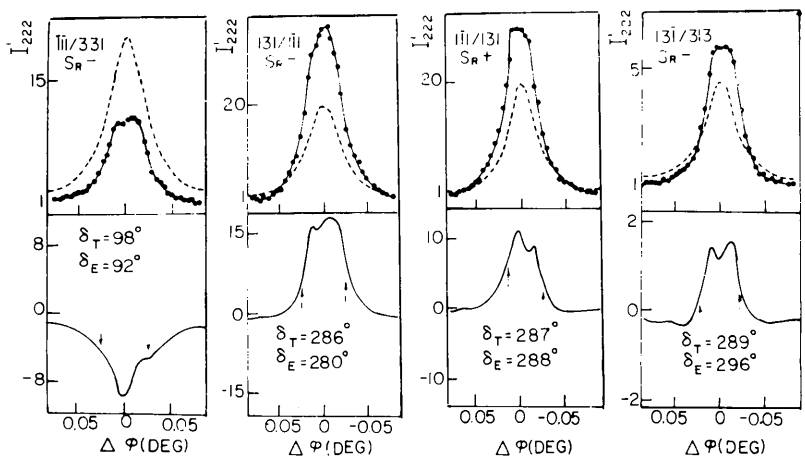

Fig. 4. Intensity profiles I'_{222} *versus* $\Delta\varphi$ for Cu $K\alpha_1$: the total profiles (the upper solid curves), the kinematical profiles (the dashed curves) and the dynamical profiles I_d (the lower solid curves).

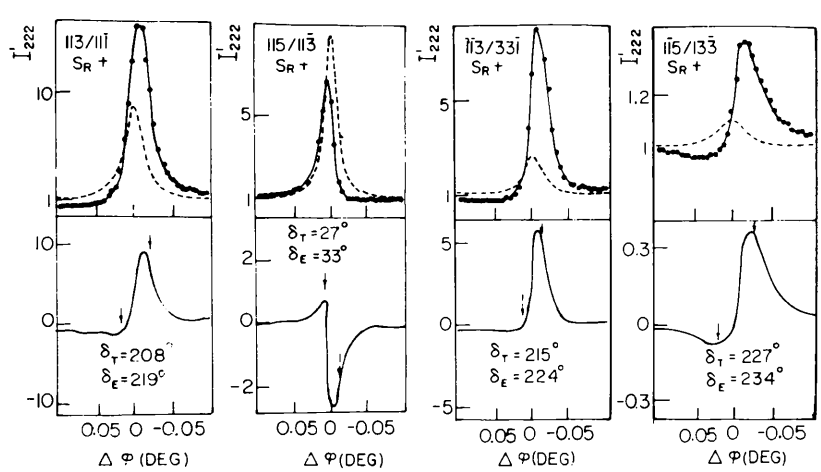

Fig. 5. Intensity profiles I'_{222} *versus* $\Delta\varphi$ for $\lambda = 1{\cdot}1236$ Å: the total profiles (the upper solid curves), the kinematical profiles (the dashed curves) and the dynamical profiles (the lower solid curves).

Table 1. *Experimental conditions*

λ (Å)	1·1236	1·5405
C_0	3·30	0·91
η_B (°)	0·06	0·04
η_M (°)	≤0·01	≤0·01

Table 2. *Experimentally determined phases for* GaAs ($G=222$) (*the subscripts E and T stand for experimental and theoretical*)

$L/G-L$	S_R	δ_E (°)	δ_T (°)	$\delta_E-\delta_T$ (°)
(1) $\lambda=1{\cdot}1236$ Å				
$113/11\bar{1}$	+	219	208	+11
$115/11\bar{3}$	+	33	27	+6
$\bar{1}\bar{1}3/33\bar{1}$	+	226	215	+11
$1\bar{1}5/13\bar{3}$	+	214	227	+13
(2) $\lambda=1{\cdot}5405$ Å				
$\bar{1}\bar{1}1/331$	−	92	98	−6
$1\bar{1}1/131$	+	288	287	+1
$131/1\bar{1}1$	−	280	286	−6
$\bar{1}3\bar{1}/3\bar{1}3$	−	296	289	+7
$\bar{5}13/71\bar{1}$	−	99	98	+1
$1\bar{1}5/13\bar{3}$	+	284	291	−7
$\bar{1}53/33\bar{1}$	−	98	104	−6
$\bar{5}31/7\bar{1}1$	−	291	295	−4
$\bar{1}1\bar{1}/313$	−	96	97	−1

curves) and the difference between these two profiles, the dynamical profiles (the lower solid curves) for the conventional and synchrotron (SR) experiments, respectively. The signs S_R of the Lorentz factors are also indicated in these two figures. As has been discussed in paper I, intensity profiles of negative S_R have to be reversed with respect to $\Delta\varphi=0$ prior to the profile analysis. The parameters used for the profile analysis are given in Table 1. The dynamical diffraction intensities $I_\pm$ at the positions $\Delta\varphi=\pm\eta_T/2$, marked with arrows in Figs. 4 and 5, are then used to determine the phase δ *via* equations (32) and (33) of paper I. The experimentally determined phases are summarized in Table 2.

IV. Discussion and concluding remarks

From paper I, the ratio between equations (32) and equation (33) leads to

$$\tan(\delta+135°)=I_+/I_-, \tag{4}$$

where I_+ and I_- are the dynamical intensities at $\Delta\varphi=\pm\eta_T/2$. Differentiating (4) with respect to δ, we obtain

$$\Delta\delta=[1+\tan^2(\delta+135°)]^{-1}\Delta(I_+/I_-) \tag{5}$$

or

$$\Delta\delta=\frac{1}{1+(I_+/I_-)^2}\left(\frac{I_+}{I_-}\right)\left(\frac{\Delta I_+}{I_+}+\frac{\Delta I_-}{I_-}\right). \tag{6}$$

This means that the error in δ is determined by the errors, ΔI_+ and ΔI_-, in I_+ and I_- respectively. According to the phase determination procedure stated above, the errors in I_+ and I_- are mainly due to the scaling factor C_0.

Table 3. *Errors in* I_P, I_K *and* C_0

$L/G-L$	$(\Delta I_P/I_P)_P$	$(\Delta I_P/I_P)_C$	$\Delta I_K/I_K$	$\overline{(\Delta C_0/C_0)}$
(1) $\lambda=1{\cdot}1236$ Å				
$113/11\bar{1}$	0·093	0·01	0·016	
$115/11\bar{3}$	0·043	0·01	0·066	0·15
$\bar{1}\bar{1}3/33\bar{1}$	0·082	0·01	0·020	
$1\bar{1}5/13\bar{3}$	0·146	0·01	0·079	
(2) $\lambda=1{\cdot}5405$ Å				
$\bar{1}\bar{1}1/331$	0·012	0·01	0·004	
$1\bar{1}1/131$	0·023	0·01	0·003	0·03
$131/1\bar{1}1$	0·021	0·01	0·006	
$\bar{1}3\bar{1}/313$	0·014	0·01	0·004	

From (1) and Fig. 3, C_0 is determined by the ratio I_P/I_K over all the three-beam cases considered. I_P and I_K are the experimental peak intensity and the calculated kinematical intensity, respectively. The error in C_0, *i.e.* $\Delta C_0/C_0$, is therefore equal to the sum of $\Delta I_K/I_K$ and $\Delta I_P/I_P$. The former is due to the theoretical approximation in the intensity calculation, the latter results from the counting statistics $\Delta I_P/I_P|_C$ and the error $\Delta I_P/I_P|_P$ in the determination of the kinematical peak positions. These errors are discussed below.

(1) *Theoretical approximation*

In the derivation of the diffraction intensity I'_G of equation (26) in paper I, the first-order approximation was employed. The higher-order terms of χ were neglected. The error in the calculated intensity due to this omission can be approximately estimated from the second-order terms. From Appendix B of paper I, the kinematical intensity errors ΔI_K can be calculated as

$$\Delta I_K=B_2^2[B_2'^2(B_0^2+B_3^2)-2B_0B_2'] \tag{7}$$

for the SR experiments and

$$\Delta I_K=B_1^2[B_2'^2(B_0^2+B_3^2+B_4'^2+B_5'^2)-2B_2'^2(B_0+B_5'\cos 2\theta)]/2 \tag{8}$$

for the conventional experiments. The errors $\Delta I_K/I_K$ for the SR and the conventional experiments are listed in Table 3. They do not exceed 10%.

(2) *Counting statistics*

In all the peak intensity measurements, the counting rate is kept in such a way that the error $\Delta I_P/I_P|_C$ is less than 1%.

(3) *Peak position*

The experimental error in determining the kinematical peak position ($\Delta\varphi=0$) is determined by the accuracy in the azimuthal scan and the angular correction due to the index of refraction of X-rays in the crystal. In the conventional experiments ($\lambda=1{\cdot}5405$ Å), the accuracy in the azimuth angle is equal to one half of the scan step, *i.e.* ±0·005°. The error

Table 4. *Experimental errors in intensity measurements and phase determination*

Case	ΔI_+	ΔI_-	I_+/I_-	$\Delta I_+/I_+ + \Delta I_-/I_-$	$\Delta\delta_E$
(1) $\lambda = 1{\cdot}1236$ Å					
$113/11\bar{1}$	0·63	0·63	0·10	0·80	4
$115/11\bar{3}$	0·76	0·76	0·21	1·25	14
$\bar{1}\bar{1}3/33\bar{1}$	0·10	0·16	0·02	1·04	1
$1\bar{1}5/13\bar{3}$	0·06	0·06	0·16	0·41	4
(2) $\lambda = 1{\cdot}5405$ Å					
$\bar{1}\bar{1}1/331$	0·48	0·48	1·07	0·15	4
$1\bar{1}1/131$	0·36	0·36	1·92	0·14	3
$131/1\bar{1}1$	0·28	0·33	1·43	0·09	2
$\bar{1}3\bar{1}/313$	0·08	0·08	2·92	0·27	4

in the ψ scan of the SR experiments is about $\pm 0{\cdot}003°$. Since the angular correction of the index of refraction is much smaller than $0{\cdot}003°$, only the errors caused by the scanning inaccuracy are considered. The errors in the intensity I_P, *i.e.* $\Delta I_P/I_P|_P$, corresponding to this scanning inaccuracy were determined from the intensity profiles for the three-beam cases considered. For illustration, the errors $\Delta I_P(E)/I_P(E)|_P$, $\Delta I_P(E)/I_P(E)|_C$, $\Delta I_K/I_K$ and the average $\overline{\Delta C_0/C_0}$ of some of the three-beam cases analyzed are listed in Table 3. The errors in δ_E, $\Delta\delta_E$, are determined according to (6), where the intensities I_+ and I_- and the variations ΔI_+ and ΔI_- are determined from the curves of I_d *versus* $\Delta\varphi$ of Figs. 4 and 5. In Table 4, the intensity measurements ΔI_+, ΔI_-, I_+/I_- and $\Delta\delta_E$ are given. Evidently, the errors $\Delta\delta_E$ of Table 4 and the differences $\delta_E - \delta_T$ of Table 2 for the SR experiments are larger than those for the conventional experiments. As is shown in Table 2, the determined phases are around 45 or 225° for $\lambda = 1{\cdot}1236$ Å and 90 and 270° for $\lambda = 1{\cdot}5405$ Å. This indicates that the error $\Delta\delta$ in this phase determination procedure is phase dependent. This is in agreement with (5), which implies that small errors in I_+/I_- near $\delta = 45$ and 225° cause large errors in δ, and that near $\delta = 135$ and 315°, the determined phase δ is almost insensitive to the errors in I_+/I_-.

Other factors which may affect the accuracy in this phase determination procedure are also examined. These include the $K\alpha_1$-$K\alpha_2$ doublet effect and the choice of distributions for the crystal mosaic spread and instrumental broadening.

(*a*) $K\alpha_1$-$K\alpha_2$ *doublet effect*

In the conventional experiment, the Cu $K\alpha_1$ and $K\alpha_2$ doublet always introduces errors in the profile analysis. Since the angular separation in θ_G of the 222 reflection between $K\alpha_1$ and $K\alpha_2$ is $0{\cdot}083°$, pinhole *A*, with the beam divergence of $0{\cdot}033°$, can well resolve this doublet. However, with the beam divergence of $0{\cdot}055°$ from pinhole *B*, the overlap between the $K\alpha_1$ and $K\alpha_2$ peaks cannot be avoided. This overlap then modifies the multiple diffraction profile and hence affects the phase determination. Table 5 lists the experimentally determined phases δ_E of the four three-beam diffractions of Cu $K\alpha_1$ radiation for these two pinholes. The difference in δ between the two is about $\pm 10°$.

Table 5. *Experimentally determined phases for the pinholes A and B for* Cu $K\alpha_1$

L/G-L	A (°)	B (°)	$\Delta\delta$
$\bar{1}\bar{1}1/331$	92	99	−7
$131/1\bar{1}1$	280	277	+3
$\bar{1}3\bar{1}/3\bar{1}3$	296	286	+10
$1\bar{1}1/131$	288	284	+4

Table 6. *Experimentally determined phases δ_E for Lorentzian and Gaussian distributions*

			$\delta_E/\Delta\delta$ (°)	
L/G-L	λ (Å)	δ_T (°)	Lorentzian	Gaussian
$\bar{1}\bar{1}1/331$	1·5405	98	92/−6	92/−6
$1\bar{1}1/131$	1·5405	287	288/+1	288/+1
$131/1\bar{1}1$	1·5405	286	280/−6	280/−6
$\bar{1}3\bar{1}/3\bar{1}3$	1·5405	289	296/+7	296/+7
$113/11\bar{1}$	1·1236	208	219/+11	219/+11
$115/11\bar{3}$	1·1236	27	33/+6	32/+5
$\bar{1}\bar{1}3/33\bar{1}$	1·1236	215	224/+9	223/+8
$1\bar{1}5/13\bar{3}$	1·1236	227	234/+7	234/+7

(*b*) *Lorentzian distribution versus Gaussian distribution*

We have assumed that the crystal mosaic spread and instrumental broadening distribution are Lorentzian. As a matter of fact, they are believed to behave as distributions between Lorentzian and Gaussian. To see the difference in the determined phases between Lorentzian and Gaussian, we construct a Gaussian distribution for the kinematical intensity profiles. The crystal spread and instrumental broadening are also assumed to be Gaussian. The phases are redetermined following the same procedure. For comparison, the determined phases δ_E for the Gaussian and Lorentzian are listed in Table 6. The differences in δ_E between the two distributions are very small.

In conclusion, we have demonstrated that with the proper choice of an incident beam divergence, the correct determination of the scaling factor and good counting statistics, the procedure stated above can be used for experimental determination of X-ray reflection phases.

The authors are indebted to the National Science Council for financial support through grant NSC 77-0208-M007-71.

References

CHANG, S.-L. & TANG, M.-T. (1988). *Acta Cryst.* **A44**, 1065-1072.
COLE, H., CHAMBERS, F. W. & DUUN, H. M. (1962). *Acta Cryst.* **15**, 138-144.

International Tables for X-ray Crystallography (1974). Vol. IV. Birmingham: Kynoch Press. (Present distributor Kluwer Academic Publishers, Dordrecht.)

KUPČIK, V., WULF, R., WENDSCHUH, M., WOLF, A. & PAEHLER, A. (1983). *Nucl. Instrum. Methods*, **208**, 519-522.

RENNINGER, M. (1937). *Z. Phys.* **106**, 141-176.

Acta Cryst. (1988). A**44**, 1078-1082

Determination of Planar Group Orientation in Patterson Methods

BY C. C. WILSON

Neutron Division, Rutherford Appleton Laboratory, Chilton, Didcot, Oxon OX11 0QX, England

AND P. TOLLIN

Carnegie Laboratory of Physics, University of Dundee, Dundee DD1 4HN, Scotland

(*Received* 8 *February* 1988; *accepted* 27 *June* 1988)

Abstract

An adaptation of the $I(\theta, \varphi)$ function for location of planar group orientation is presented. More accurate determination of this orientation is found to be possible in some cases using the modified functions, based on rings and hoops rather than disks in Patterson space. In some examples incorrect orientations are corrected by the new functions. A possible extension to the simultaneous detection of several small group orientations in one molecule, based on bond length selection, is discussed.

Introduction

The $I(\theta, \varphi)$ function was defined by Tollin & Cochran (1964). The philosophy of the function is to recognize that in a planar group the vectors between pairs of atoms in that group will all lie in one plane in Patterson space. By placing a disk of dimensions approximating to those of the planar group at the origin in Patterson space, one can rotate this disk in the two spherical polar coordinates θ and φ, the integral of the Patterson function over the disk being maximized when the disk is in the same orientation as the planar group.

The $I(\theta, \varphi)$ function is

$$I(\theta, \varphi) = \int_{\mathbf{r}} P(\mathbf{r}) t(\mathbf{r})\, d\mathbf{r} \qquad (1)$$

where

$$t(\mathbf{r}) = \begin{cases} 1 & \text{on disk} \\ 0 & \text{elsewhere.} \end{cases}$$

One may use the facts that the transform of $P(\mathbf{r})$ is $|F(\mathbf{h})|^2$ and that of a disk is related to the first-order Bessel function $J_1(x)$ and exploit Parseval's theorem to evaluate this (apart from constant factors) as

$$I(\theta, \varphi) = \sum_{\mathbf{h}} |F_{\mathbf{h}}|^2 2\pi R^2 J_1(2\pi RS)/2\pi RS \qquad (2)$$

where S is the distance of the reciprocal-lattice point $\mathbf{h}$ from the normal to the disk, R is the disk radius, and $J_1(x)$ is the first-order Bessel function. In practice the $|F_{\mathbf{h}}|^2$ values are replaced by sharpened structure factors $|F^s_{\mathbf{h}}|^2$ in the calculations.

Since its definition, this function has been found to locate the orientation of planar groups with accuracy in many cases. However, there are occasions when the located orientation is either very inaccurate or incorrect when $I(\theta, \varphi)$ is calculated.

Investigation of cases where these problems have arisen has suggested three possible contributing factors.

(1) Overemphasis of the contributions of some high-order [high $(\sin\theta)/\lambda$] reflections, caused by the sharpening procedure applied to the $|F_{\mathbf{h}}|^2$.

(2) Possible asymmetry in the large origin peak in the Patterson function, especially in cases where the asymmetric unit is large and only a small portion is planar.

(3) When the orientation of the group is close to one of the extrema of the $I(\theta, \varphi)$ function (*e.g.* close to $\theta = 90°$) an 'averaged' orientation of the group and a symmetry-related group may be found. For example in the TAA example (below) the correct θ value is $\sim 80°$, but the $I(\theta, \varphi)$ indicates $\sim 90°$ - in this orthorhombic example there is also a peak at $\theta \sim 100°$, by symmetry. This ambiguity is caused by intergroup vectors.

The simplest way of dealing with factor (1) is to use data from a restricted range of $(\sin\theta)/\lambda$ as used in other Patterson-methods techniques (Wilson & Tollin, 1988), but in this case cutting off the outer [higher $(\sin\theta)/\lambda$] data. The use of $|E_{\mathbf{h}}|^2$ values does not in general eliminate oversharpening problems, as noted elsewhere (Wilson & Tollin, 1988). Problems can be encountered in trying to eliminate factor (2) by attempting to remove a particularly large and asymmetric origin peak from the Patterson function

0108-7673/88/061078-05$03.00